

## Vacuum-mediated multiphoton transitions

J. R. Bochinski,\* C. C. Yu,† T. Loftus, and T. W. Mossberg

Oregon Center for Optics and Department of Physics, University of Oregon, Eugene, Oregon 97403

(Received 17 August 2000; published 9 April 2001)

We have measured the emission spectra of two-level-like atoms driven by a spatially inhomogeneous bichromatic field comprised of one resonant and one off-resonant component. Under these excitation conditions, observed spectra consist of several narrow peaks appearing on top of a broad continuumlike structure. This experimental approach provides for selective observation of those spectral features having a Rabi-frequency-independent emission frequency. Such emission processes involve multiphoton transitions, with one leg being spontaneous, between dressed-state levels differing only in their photonic quantum numbers; i.e., between equivalent dressed-state-doublet sublevels. Related vacuum-mediated transitions have recently been invoked as an underlying mechanism of inversionless gain.

DOI: 10.1103/PhysRevA.63.051402

PACS number(s): 32.80.Wr, 42.50.Hz, 33.80.Wz

The emission spectra of two-level atoms (TLAs) driven by strong, spatially homogeneous, near-resonant, monochromatic radiation can be qualitatively motivated using the dressed atom model. As shown in Fig. 1(a), the spectrum forms a symmetric, Mollow triplet structure [1] centered at the driving field frequency with central to sideband peaks separation given by the generalized Rabi frequency  $\Omega_1^G$ , defined as

$$\Omega_1^G = \sqrt{\Omega_1^R{}^2 + \Delta_1^2} \quad (1)$$

where  $\Omega_1^R$  is the resonant Rabi frequency, and  $\Delta_1 = \nu_1 - \nu_a$  is the detuning of the excitation field frequency  $\nu_1$  from the atomic resonance frequency  $\nu_a$ . Figure 1(b) schematically depicts how the splitting of the dressed ladder levels  $\Omega_1^G$  increases with  $|\Delta_1|$ . The spectral features are intuitively motivated as transitions between atom+field eigenstates (dressed states). Figure 1(c) shows allowed single-photon transitions between pairs of adjacent dressed doublet sublevels. The composite states are defined in the usual manner [2]:

$$|1(N)\rangle = \sin \theta |g, N+1\rangle + \cos \theta |e, N\rangle, \quad (2)$$

$$|2(N)\rangle = \cos \theta |g, N+1\rangle - \sin \theta |e, N\rangle, \quad (3)$$

where  $N$  is the photonic quantum number,  $g(e)$  is the unperturbed ground (excited) atomic state, and  $\theta$  is given as

$$\tan(2\theta) = -\frac{\Omega_1^R}{\Delta_1}, \quad 0 \leq 2\theta < \pi. \quad (4)$$

The theory of TLAs in the presence of homogeneous bichromatic excitation fields has received some attention [3,4]. Absorptive experiments have revealed effects such as Rabi subharmonic resonances [5] and the generation of novel gain and loss features [6]. Fluorescence measurements under

symmetric (asymmetric) bichromatic driving fields, where spectral components are equally (unequally) detuned from the atomic transition frequency, in both continuous-wave (cw) and transient regimes have demonstrated a variety of complex phenomena and generated new insights into the underlying light-matter interactions [7,8]. For example, a recent experiment measured complicated, multi-peaked spectra that are well modeled by doubly dressing the bare atom [4,8]. Interestingly, further exploration of this system may demonstrate the dynamical suppression of spontaneous emission via quantum interference between dressed-state transitions [9].

In the work presented here, we observe emission spectra displayed by TLAs under strong, spatially *inhomogeneous*, cw, bichromatic excitation with one resonant ( $\nu_1$ ) and one off-resonant ( $\nu_2$ ) field component. The inhomogeneous field experiment of interest here differs from typical measurements wherein the pump fields are made spatially homoge-

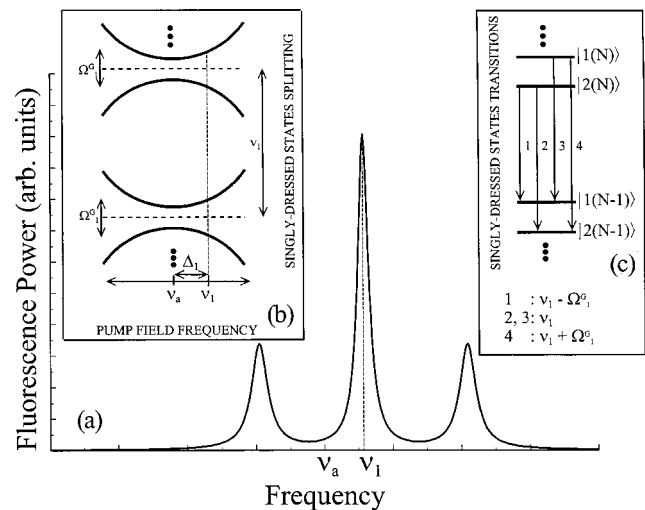


FIG. 1. (a) Calculated fluorescence spectrum of a TLA under a strong, monochromatic spatially uniform excitation:  $\Omega_1^R \sim 150$  MHz,  $\Delta_1 \sim 55$  MHz, and  $\Gamma = 19$  MHz. (b) Dressed-state splitting increases as  $\Delta_1$  is varied. (c) Allowed single-photon transitions (solid arrows) between pairs of adjacent dressed-state sublevel doublets.  $\Omega_1^G$ , generalized Rabi-frequency;  $\nu_1$ , pump field frequency;  $\nu_a$ , atomic resonance frequency;  $\Delta_1$ , pump field detuning.

\*Present address: JILA, University of Colorado at Boulder, Boulder, CO 80309-0440.

†Present address: George R. Harrison Spectroscopy Laboratory, Massachusetts Institute of Technology, Cambridge, MA 02139.

neous so that excitation Rabi frequencies have unique values. Inhomogeneous fields, on the other hand, provide a continuum of Rabi frequencies, smearing away spectral peaks whose positions are Rabi-frequency-dependent. Only those spectral peaks having Rabi-frequency-independent locations survive, thereby simplifying the spectrum and isolating certain transition types. Contrasting spectra obtained with spatially uniform excitation with those obtained with spatially inhomogeneous excitation provides a useful tool in understanding complex multifield excitation spectra.

The spectrally sharp features that remain derive from hyper-Raman processes coupling dressed levels differing only in photonic quantum numbers. Such transitions are usefully modeled as multiphoton transitions including a vacuum-mediated (spontaneous) decay step. Remarkably, even in the presence of strong driving fields, these particular processes can also be described in the bare-state basis. Additionally, we note that the irreversible nature of the spontaneous-emission event in these multiphoton transitions breaks the absorption-emission symmetry [10] and allows for potential creation of inversionless gain. While the same two-level driven system supports various parametric gain processes, true laser gain can be identified through its phase insensitivity and ability to “condense” excitation from a broad spectrum into monochromatic output.

The experiment uses a collimated beam (0.75 mm diameter) of two-level-like barium (Ba) atoms in natural abundance from an effusion oven. The atomic beam passes through the center of a 5-cm confocal Fabry-Perot cavity, where it is intersected by an excitation field consisting of one or two spectral components. The cavity axis, laser, and atomic beams are mutually orthogonal. The piezoelectrically scannable cavity gathers and spectrally filters fluorescence, which is detected, after spatial and angular filtering optics, by a photomultiplier tube (PMT). Spectra are measured by monitoring the light power emitted out one end of the cavity as a function of cavity length and therefore cavity transmission frequency  $\nu$ . Only a single cavity mode falls within the atomic emission profile. The spectral sweep rate of the cavity mode  $d\nu/dt$  varies by less than 3%, introducing corresponding nonlinearity in observed spectra. The cavity has a free spectral range ( $c/4L$ ) of 1500 MHz and a finesse of  $\sim 500$ .

In our experiments, the linearly polarized output of a single-mode cw, ring dye laser (RDL) at frequency  $\nu_1$  is frequency-locked via saturation spectroscopic techniques to  $\nu_a$ , the frequency of the  $(6s^2) ^1S_0 - (6s6p) ^1P_1$  transition (natural width  $\Gamma = 19$  MHz) of nuclear-spin-free  $^{138}\text{Ba}$  [Fig. 2(a)]. An acousto-optic modulator (AOM) is used to create [Fig. 2(b)] the second driving field component with frequency  $\nu_2 = \nu_1 - 2\Delta_{\text{RF}}$ , where  $\Delta_{\text{RF}} = 80$  MHz is the AOM drive frequency. We define the frequency difference between the two field components  $\delta = \nu_1 - \nu_2 = 2\Delta_{\text{RF}} = 160$  MHz. The bichromatic driving field is spatially separated from the monochromatic beam input to the AOM by a polarization beam-splitter cube (PBS). An electric-optic modulator (EOM) acts as a variable waveplate that, combined with the polarization selectivity of the PBS, enables variable amplitude control of the  $\nu_2$  driving field component. The excita-

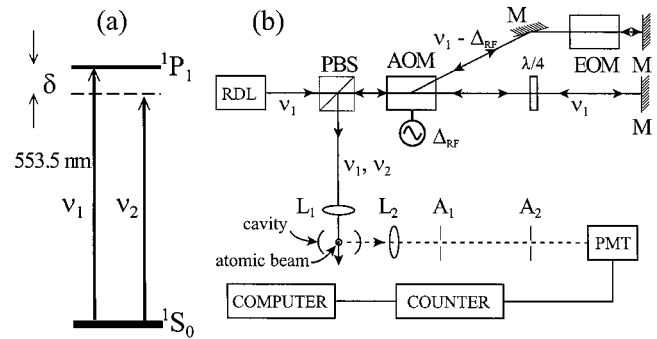


FIG. 2. (a) The  $(6s^2) ^1S_0 - (6s6p) ^1P_1$  transition at 553.5 nm in  $^{138}\text{Ba}$  is a two-level-like system:  $\nu_1$ , resonant pump field component;  $\nu_2$ , off-resonant pump field component;  $\delta = \nu_a - \nu_2$ . (b) Experimental schematic: RDL, ring dye laser; PBS, polarization beam splitter; AOM, acousto-optic modulator; M, mirror;  $\lambda/4$ , quarter-wave plate; EOM, electro-optic modulator; L1, focusing lens; PL, polarizer; L2, lens; A1 and A2, apertures; PMT, photomultiplier tube;  $\Delta_{\text{RF}}$ , AOM drive signal.

tion beam may be collimated (focused) as it intersects the atomic beam, creating a spatially homogeneous (inhomogeneous) excitation field. Collimated beams of the diameter employed here do not provide perfectly uniform excitation. It is the large contrast with the focused excitation case that provides useful input regarding the nature of observed spectral peaks. Note, retroreflecting the pump laser beam and creating a standing-wave-like pump offers an alternative means to create the inhomogeneous excitation condition.

When probed by a weak, collimated, orthogonally propagating, monochromatic laser field, the atomic beam displays an absorptive linewidth of  $\sim 21$  MHz on the  $^{138}\text{Ba}$  transition, with the excess width as compared to  $\Gamma$  attributed to the angular spread of the atomic beam and excitation laser linewidth. It is estimated that the saturation locking scheme maintains  $|\nu_1 - \nu_a| < 3$  MHz, where deviation from exact orthogonality of the excitation and atomic beams contributes the primary detuning uncertainty. Emission spectra exhibit an instrumental resolution  $\Gamma_c \sim 13$  MHz limited by finite cavity resolution and residual atomic beam Doppler broadening.

Figure 3 shows a series of fluorescence spectra of TLAs driven by a strong resonant ( $\nu_1 \approx \nu_a$ ) monochromatic pump field. Trace (i) depicts the classic Mollow triplet spectrum predicted for a spatially homogeneous resonant Rabi frequency of  $\Omega_1^R \sim 200$  MHz [1], while trace (ii) shows experimental results obtained under the same spatially homogeneous excitation, revealing primarily the influence of finite experimental resolution. Some slight additional broadening of the sidebands occurs due to off-resonant excitation of non- $^{138}\text{Ba}$  isotopes [8] and residual excitation-field inhomogeneity. Trace (iii) illustrates the measured spectrum produced using spatially inhomogeneous excitation (i.e., focused driving field). The sideband peaks are strongly broadened, producing continuumlike shoulders. Peak field intensity has increased such that the maximum  $\Omega_1^R = 350$  MHz.

Addition of a second driving field component to the focused excitation beam produces a variety of interesting spectra. In the following, we hold the power of the resonant ex-

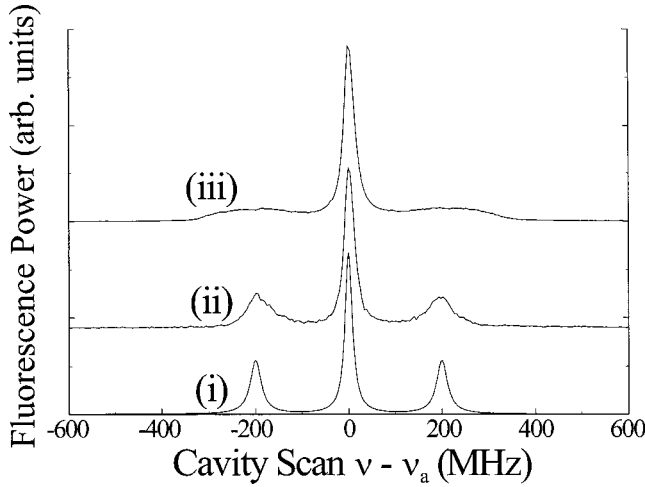


FIG. 3. Fluorescence power vs cavity detuning from the atomic transition frequency ( $\nu - \nu_a$ ). (i) Calculated spectra under resonant, monochromatic, spatially homogeneous excitation,  $\Omega_1^R \sim 200$  MHz. (ii) Experimental result for resonant homogeneous excitation. (iii) Same as (ii) with pump beams having the same integrated power, but with a highly nonuniform spatial profile,  $\Omega_1^R$  maximum  $\sim 350$  MHz.

citation field component constant, producing a maximum  $\Omega_1^R = 350$  MHz, and vary the power, and hence, the maximum Rabi frequency  $\Omega_2^R$ , of the second driving field component. In Fig. 4(a),  $\Omega_2^R = 0$  MHz. The dominant feature of the spectrum, a sharp peak at  $\nu - \nu_a = 0$  results primarily from elastic scattering of the resonant pump field component. In Fig. 4(b), maximum  $\Omega_2^R = 150$  MHz and application of the second excitation field component imbalances the broad spectrum, introducing peaks at  $\nu - \nu_a = -\delta$ ,  $\delta$ , and  $2\delta$ . Moreover, the central peak develops a wing extending toward lower frequencies. Solid arrows mark the spectral loca-

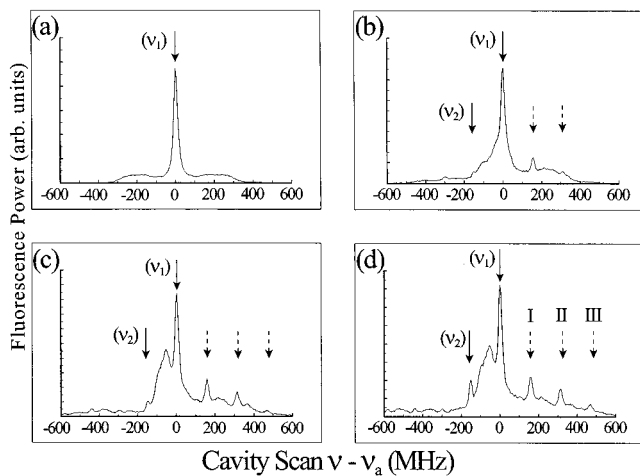


FIG. 4. Measured fluorescence power vs cavity detuning ( $\nu - \nu_a$ ). Solid arrows indicate frequencies of the resonant ( $\nu_1$ ) and off-resonant ( $\nu_2$ ) driving field components. Dashed arrows mark hyper-Raman peaks at  $\nu_s = \nu_1 + m\delta$ , for  $m=1,2,3$ .  $\delta=160$  MHz, maximum  $\Omega_1^R \sim 350$  MHz, and maximum  $\Omega_2^R$  varies. (a) Maximum  $\Omega_2^R = 0$  MHz, (b) 150 MHz, (c) 250 MHz, and (d) 350 MHz.

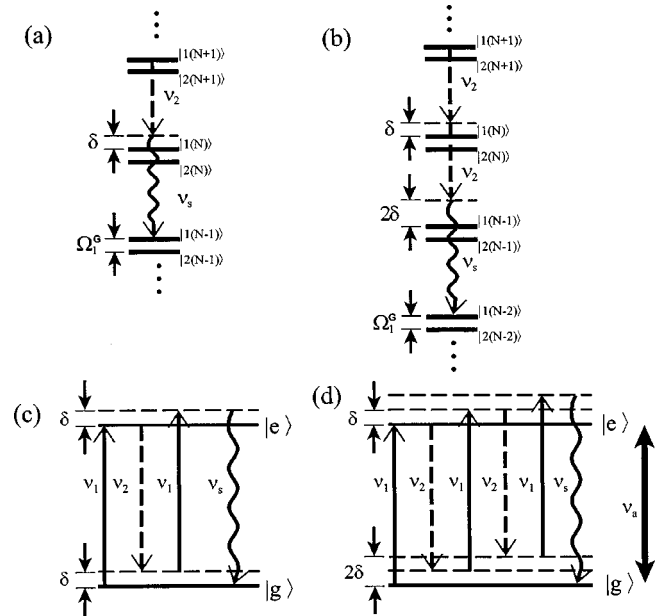


FIG. 5. Hyper-Raman processes. Dressed-state basis: (a) two-photon processes; (b) three-photon process. Bare state basis: (c) four-photon process; (d) six-photon process.  $\nu_1$ , resonant pump photon (solid arrow);  $\nu_2$ , off-resonant pump photon (dashed arrow);  $\nu_s$ , spontaneously emitted photon (wavy arrow);  $\nu_a$ , atomic transition frequency;  $\Omega_1^G$ , generalized Rabi frequency off-resonant field component;  $\delta = \nu_a - \nu_2$ . The horizontal dashed lines are virtual states.

tions of the excitation field components. Dashed arrows indicate prominent new spectral components. In Fig. 4(c), the maximum of  $\Omega_2^R$  is increased to 250 MHz and the generated spectral peaks grow in height. Additionally, a small feature at  $\nu - \nu_a = 3\delta$  emerges. Note the wide large feature whose peak falls at  $\nu - \nu_a = -55$  MHz is actually a smeared Rabi-dependent structure [8,11]. In Fig. 4(d),  $\Omega_1^R = \Omega_2^R = 350$  MHz and induced Rabi-independent peaks are even more pronounced.

The sharp features in the fluorescence spectra can be described in terms of multiphoton, hyper-Raman processes whose single spontaneous decay step generates the observed peaks. The lowest-order mechanism appears in the dressed-state basis as a two-photon transition. Allowing the strong resonant pump driving field  $\nu_1$  to dress the atom as in Fig. 5(a) and starting in the upper sublevel of the dressed atom doublet, a stimulated emission step induced by  $\nu_2$  (dashed arrow) is followed by vacuum-mediated emission (wavy arrow) at frequency  $\nu_s = \nu_1 + \delta$ . Due to dressed-state symmetry, starting in either dressed doublet sublevel produces spontaneously emitted photons of the same frequency. Figure 5(b) depicts the next higher multiphoton process involving two stimulated photons at  $\nu_2$  resulting in the spontaneous photon at  $\nu_s = \nu_1 + 2\delta$ . Generalizing, fluorescence at  $\nu_s = \nu_1 + m\delta$  ( $m=1,2,\dots$ ) is generated by  $m$  stimulated emissions at  $\nu_2$ . Importantly, the multiphoton processes just described produce emission frequencies independent of excitation field Rabi frequencies because they couple equivalent dressed-state doublet sublevels. The process depicted in Figs. 5 (a)

[Fig. 5(b)] produces the I (II) peak shown in Fig. 4(d), while the next order process generates the III peak.

Despite the presence of the strong driving fields, these multiphoton emission processes can also be described in the bare-state basis. In the bare-state basis, fluorescence at  $\nu_s = \nu_1 + m\delta$  is generated by the absorption of  $m+1$  photons at frequency  $\nu_1$  combined with the stimulated emission of  $m$  photons at frequency  $\nu_2$ . Figure 5(c) depicts a bare-state description of the dressed-state process shown in Fig. 5(a). Two absorbed resonant photons at  $\nu_1$  (solid arrows), a stimulated photon at  $\nu_2$  (dashed arrow), combine to yield a spontaneous photon at frequency  $\nu_s = \nu_1 + \delta$  (wavy arrow). Figure 5(d) provides a bare-state description of the Fig. 5(b) dressed-state process. Note that transitions coupling non-equivalent components of the dressed-state doublets produce Rabi-dependent spectral peaks. Such peaks are discrimi-

nated against using spatially inhomogeneous excitation fields.

The processes whose signatures are reported here possess both a stimulated emission and vacuum-mediated (spontaneous) decay step, and have been suggested as a means to generate inversionless gain [10]. The use of inhomogeneous excitation fields represents an enabling experimental approach for isolating these transitions from the multiple peaks generated by multichromatic excitation. Direct experimental verification that these processes support inversionless gain remains a challenging task. However, the unambiguous observation of the multiphoton transitions lends tantalizing support for these concepts.

We gratefully acknowledge financial support from the National Science Foundation under Grant No. PHY-9870223.

- 
- [1] B. R. Mollow, Phys. Rev. **188**, 1969 (1969); F. Schuda, C. R. Stroud, Jr., and M. Hercher, J. Phys. B **7**, L198 (1974); W. Hartig, W. Rasmussen, R. Schnieder, and H. Walther, Z. Phys. A **278**, 205 (1976); R. E. Grove, F. Y. Wu, and S. Ezekiel, Phys. Rev. A **15**, 227 (1977).
- [2] C. Cohen-Tannoudji and S. Reynaud, J. Phys. B **10**, 345 (1977); C. Cohen-Tannoudji, J. Dupont-Roc, and G. Grynberg, *Atom-Photon Interactions* (John Wiley and Sons, New York, 1992), pp. 410–426.
- [3] R. Guccione-Gush and H. P. Gush, Phys. Rev. A **10**, 1474 (1974); S. P. Goreslavsky, N. B. Delone, and V. P. Krainov, J. Phys. B **13**, 2659 (1980); V. Hizhnyakov and M. Rozman, Opt. Commun. **52**, 183 (1984); G. S. Agarwal and N. Nayak, J. Opt. Soc. Am. B **1**, 164 (1984); G. Yu. Kryuchkov, Opt. Commun. **54**, 19 (1985); G. S. Agarwal and N. Nayak, Phys. Rev. A **33**, 391 (1986); M. Wilkens and K. Rzazewski, *ibid.* **40**, 3164 (1989); H. Freedhoff and Z. Chen, *ibid.* **41**, 6013 (1990); G. S. Agarwal, Y. Zhu, D. J. Gauthier, and T. W. Mossberg, J. Opt. Soc. Am. B **8**, 1163 (1991); G. Kryuchkyan, Zh. Eksp. Teor. Fiz. **99**, 1416 (1991) [Sov. Phys. JETP **72**, 790 (1991)]; W. M. Ruyten, J. Opt. Soc. Am. B **9**, 1892 (1992); Z. Ficek and H. S. Freedhoff, Phys. Rev. A **48**, 3092 (1993); T. G. Rudolph, H. S. Freedhoff, and Z. Ficek, *ibid.* **58**, 1296 (1998).
- [4] Z. Ficek and H. S. Freedhoff, Phys. Rev. A **53**, 4275 (1996).
- [5] S. Chakmakjian, K. Koch, and C. R. Stroud, Jr., J. Opt. Soc. Am. B **5**, 2015 (1988); W. M. Ruyten, *ibid.* **6**, 1796 (1989); S. Papademetriou, S. Chakmakjian, and C. R. Stroud, Jr., *ibid.* **9**, 1182 (1992); N. B. Manson, C. Wei, and J. P. D. Martin, Phys. Rev. Lett. **76**, 3943 (1996).
- [6] A. S. M. Windsor, C. Wei, S. A. Holmstrom, J. P. D. Martin, and N. B. Manson, Phys. Rev. Lett. **80**, 3045 (1998); J. R. Bochinski (unpublished).
- [7] Y. Zhu, Q. Wu, A. Lezama, D. J. Gauthier, and T. W. Mossberg, Phys. Rev. A **41**, 6574 (1990); Q. Wu, D. J. Gauthier, and T. W. Mossberg, *ibid.* **49**, R1519 (1994); **50**, 1474 (1994).
- [8] C. C. Yu, J. R. Bochinski, T. M. V. Kordich, T. W. Mossberg, and Z. Ficek, Phys. Rev. A **56**, R4381 (1997).
- [9] Z. Ficek and T. Rudolph, Phys. Rev. A **60**, R4245 (1999).
- [10] P. B. Sellin, C. C. Yu, J. R. Bochinski, and T. W. Mossberg, Phys. Rev. Lett. **78**, 1432 (1997).
- [11] C. C. Yu, J. R. Bochinski, and T. W. Mossberg (unpublished).